ACS APPLIED MATERIALS & INTERFACES

Letter

www.acsami.org

Antibacterial Property of Graphene Quantum Dots (Both Source Material and Bacterial Shape Matter)

Liwei Hui,[†,§] Jianliu Huang,[‡] Guanxiong Chen,[§,$] Yanwu Zhu,[§,$,¶] and Lihua Yang*[,†,§,#]

[†]CAS Key Laboratory of Soft Matter Chemistry, [§]Department of Materials Science and Engineering, [‡]Physics and Chemistry Analysis Laboratory, [$]CAS Key Laboratory of Materials for Energy Conversion, [¶]iChEM (Collaborative Innovation Center of Chemistry for Energy Materials), and [#]Department of Polymer Science and Engineering, University of Science and Technology of China, Hefei, Anhui 230026 China

Supporting Information

ABSTRACT: Whereas diverse graphene quantum dots (GQDs) with basal planes similar to those of graphene oxide sheets (i.e., GO-GQDs) lack antibacterial property, that prepared by rupturing C_{60} cage (i.e., C_{60}-GQD) effectively kills *Staphylococcus aureus*, including its antibiotic-tolerant persisters, but not *Bacillus subtilis*, *Escherichia coli*, or *Pseudomonas aeruginosa*. The observed activity may correlate with a GQD's ability to disrupt bacterial cell envelop. Surface-Gaussian-curvature match between a GQD and a target bacterium may play critical role in the association of the GQD with bacterial cell surface, the initial step for cell envelope disruption, suggesting the importance of both GQDs' source materials and bacterial shape.

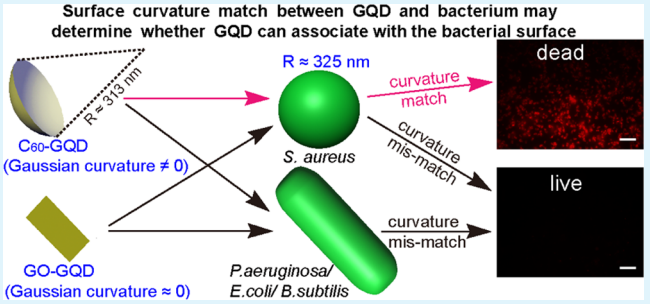

KEYWORDS: *two-dimensional material, drug-resistance, antimicrobial, fullerene, cytotoxicity*

Graphene quantum dots (GQDs) are carbon nanosheets of <20 nm in lateral dimension[1,2] and have recently attracted great research attention because of their unique spin[3] and electronic.[4] To date, GQDs have been synthesized via either the top-down strategy from various carbon materials (e.g., graphene,[5] graphene oxide (GO),[6] coal,[7] and carbon fibers[8]) or the bottom-up strategy either noncovalently from ruptured buckminsterfullerene (C_{60})[9,10] or covalently from, for example, glucose[11] and benzene-derivatives.[12] Despite mounting investigations on GQDs, systematic examination on their antibacterial property is still lacking. Absence of information on this aspect appears to be even more regretful when considering the extensive investigations on the antibacterial property of other carbon nanomaterials including graphene and GO sheets,[13] carbon nanotubes,[14] and aqueous dispersion of C_{60} cage.[15] Scattered evidence shows that in suspension, GQD prepared from GO sheets (i.e., GO-GQD) is inactive against a wide-spectrum of bacteria,[16,17] despite of the wide-spectrum antibacterial activity of GO sheets (usually several tens to hundreds of nanometers in lateral dimension).[13] Similar inactivity is observed with GQD prepared from graphite rods,[18] which is also called GO-GQD likely because of its similar basal plane structure as GO sheets. On the basis of these observations, one may intuitively assume that all GQDs lack antibacterial property. Is this really the case? Before addressing this question, let us first look whether all GQDs are the same. Among the diverse source materials for GQDs, C_{60} is the only one that contains pentagon and hexagon arranged in specific manner, rather than hexagon alone. As a result, GQD prepared by rupturing C_{60} cage (i.e., C_{60}-GQD) may inherit nonzero Gaussian curvature, in contrast to the zero Gaussian curvature of GO-GQDs, which adopt a flat sheet morphology because of their small lateral dimensions. Note that surface curvature of carbon-based nanomaterials plays pivotal role in protein adsorption on their surfaces.[19] We redefine the above question with a better focus as "can fingerprint difference in structure of source materials lead to GQDs of distinct antibacterial property?" In other words, will C_{60}-GQD lack antibacterial property as do GO-GQDs, or will it exhibit wide-spectrum activity as does C_{60} cage?[15]

To address the above questions, we herein examine the antibacterial properties of C_{60}-GQD and a commercially available GO-GQD prepared via the bottom-up strategy and compare our results on these two GQDs with prior reports on antibacterial property of GO-GQDs prepared via the top-down strategy. Our C_{60}-GQD is prepared with a modified Hummers method followed by dialysis for 6 days (Figure 1a),[10] as confirmed consistently with Raman spectrum (Figure S1a), FT-IR spectrum (Figure S2a), atomic force microscopy (AFM) characterizations (Figure S3a–c), and photoluminescence spectra (Figure S4a). GO-GQD used in this work is commercially available and prepared via a bottom-up approach according to information from the vendor; upon receiving, Raman spectrum (Figure S1b), FT-IR spectrum (Figure S2b),

Received: October 25, 2015
Accepted: December 22, 2015
Published: December 22, 2015

DOI: 10.1021/acsami.5b10132
ACS Appl. Mater. Interfaces 2016, 8, 20–25

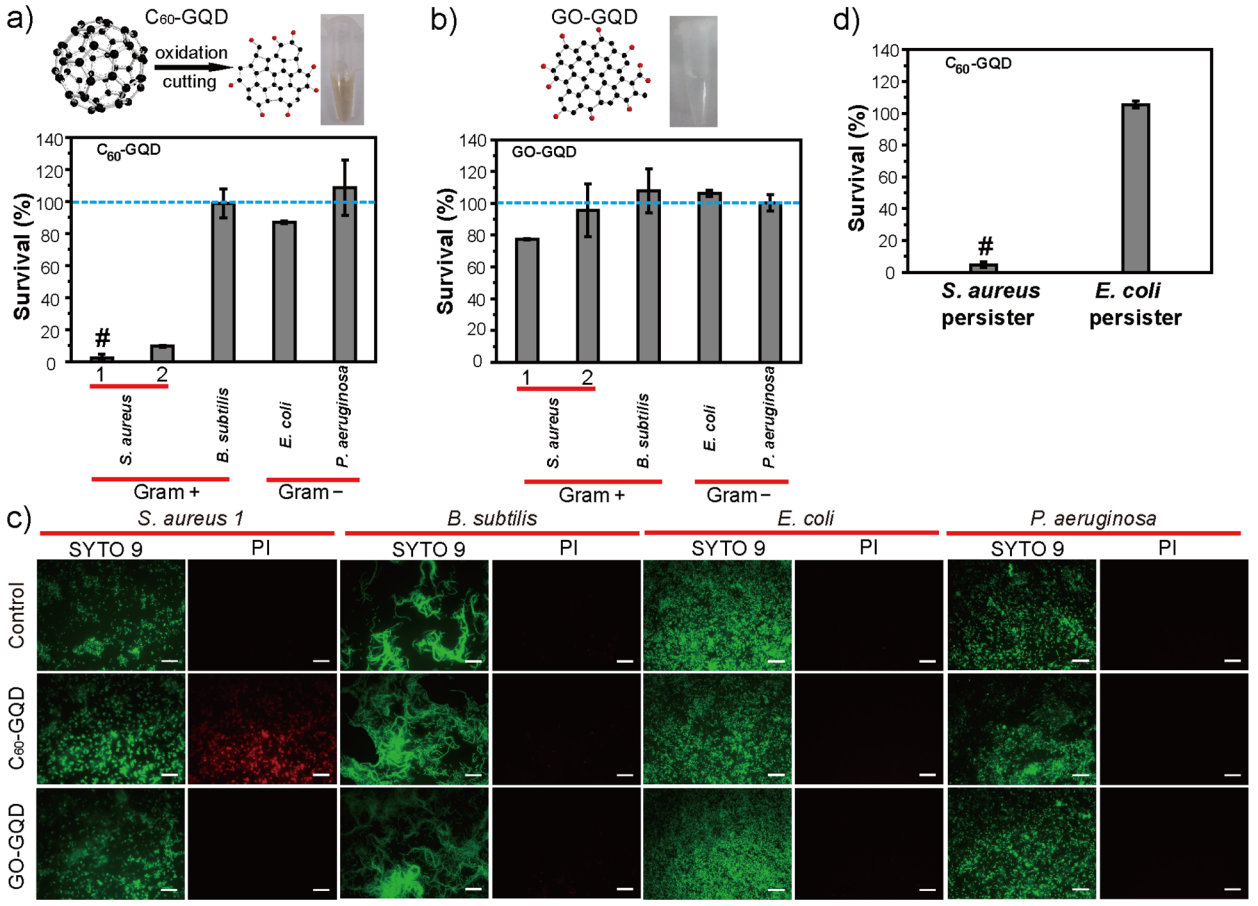

Figure 1. (a, b) Bacterial plate killing assays using (a) C_{60}-GQD and (b) GO-GQD; both GQDs are at 200 μg/mL in saline. After 3 h treatment, C_{60}-GQD significantly reduces the viability of *S. aureus* (1: ATCC 25923; 2: ATCC 29213) but barely affects that of the other three bacteria tested——*B. subtilis*, *E. coli*, *P. aeruginosa*——regardless of their Gram-property. In stark contrast, GO-GQD barely affects the survival of all five strains tested. # indicates bacterial survival ratio of <5%. Blue dash-line indicates 100% survival. Data points are reported as mean ± standard deviation. (c) Fluorescence microscopy images show that, after 3-h treatment in saline, C_{60}-GQD (400 μg/mL) renders cells of *S. aureus* stain intensely red, indicative of dead cells with compromised membranes, whereas those of *B. subtilis*, *E. coli*, *P. aeruginosa* remain dark in the red channel, indicative of live cells with healthy membranes. In stark contrast, after similar treatment with GO-GQD, all bacterial cells remain dark in the red channel, indicative of live cells. Controls are those assayed similarly but without GQD addition. Scale bar = 20 μm. (d) Bacterial plate killing assays using C_{60}-GQD (200 μg/mL) against bacterial persisters. After 3-h treatment in saline, C_{60}-GQD significantly reduces the viability ratio of *S. aureus* persisters but barely impacts that of *E. coli* persisters. Data points are reported as mean ± standard deviation. # indicated bacterial survival percentage of <5%.

AFM images (Figure S3d–-f), and photoluminescence spectra (Figure S4b) were performed to confirm its identity. Both C_{60}-GQD and GO-GQD are readily dispersible in water. The resulting dispersion of C_{60}-GQD in saline (0.9% NaCl in Millipore water) appears to be light brown while that of GQ-GQD appears to be clear; both of which are stable for several months without precipitation (Figure 1). AFM analysis reveals that C_{60}-GQD has an average lateral dimension and an average apparent sheet thickness of up-to-15 nm and 1.37 ± 0.46 nm (Figure S3b, c), respectively, consistent with prior reports.[9,10] On the other hand, the as-purchased GO-GQD exhibits an average lateral dimension and an average apparent sheet thickness of up-to-15 nm and 0.94 ± 0.29 nm (Figure S3e, f), respectively, as do GO-GQDs prepared via the top-down approaches.[6,20] X-ray photoelectron spectroscopy (XPS) characterizations suggest that C_{60}-GQD has slightly higher extent of oxidation than our GO-GQD (as indicated by the higher oxygen to carbon mass ratios) (Table S1). When dispersed in Millipore water, both C_{60}-GQD and GO-GQD exhibit negative zeta potentials, indicative of negative surface charges (Figure S5). Clearly, C_{60}-GQD and GO-GQDs exhibit high similarity in morphology, size, elemental composition, and surface charge.

Intriguingly, plate killing assays[21] reveal distinction in antibacterial activity profiles of C_{60}-GQD versus GO-GQDs (Figure 1). *S. aureus* and *B. subtilis* are used as representative Gram-positive bacteria, whereas *E. coli* and *Pseudomonas aeruginosa* (*P. aeruginosa*) as representative Gram-negative bacteria. After 3-h coincubation in saline, GO-GQD (200 μg/mL) barely impacts the viability ratios of all bacterial strains tested (Figure 1b), indicative of lack of antibacterial property, similar as do GO-GQDs prepared via the top-down strategy.[16−18] The observed inactivity of GO-GQDs may arise because availability of GO basal planes determines whether it is antibacterial[21,22] and smaller lateral dimension leads to GO sheet of weaker activity.[23] In stark contrast, our C_{60}-GQD significantly reduces the viability ratio of *S. aureus* (ATCC 25923, named *S. aureus* 1 throughout this work) (lowered to 2.3%) but barely affects those of the other three bacteria (Figure 1a), despite that *S. aureus* and *B. subtilis* are both Gram-

DOI: 10.1021/acsami.5b10132
ACS Appl. Mater. Interfaces 2016, 8, 20−25

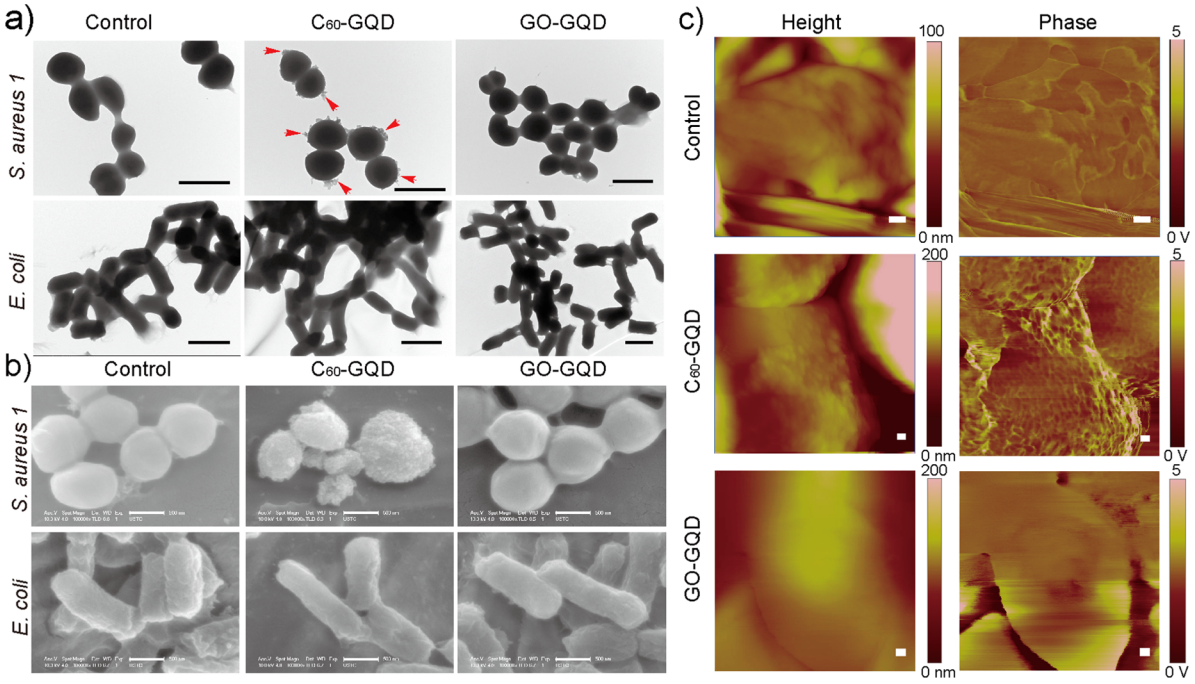

Figure 2. (a) TEM images show that surfaces of *S. aureus* cells treated with C_{60}-GQD (400 μg/mL) in saline exhibit many "tiny sticks/blebs", indicative of cell envelope destabilization, whereas those of cells treated similarly but with GO-GQD remain smooth as do those of cells in the controls, indicative of undetectable destabilization to cell envelope. Red arrows indicated the presence of "tiny sticks/blebs". In contrast, *E. coli* cells retain smooth surfaces no matter which type of GQDs was used to treat them, as do those in the controls. Controls are those assayed similarly but without GQD addition. Scale bar = 1 μm. (b) SEM images under 100 000× magnification show that surfaces of *S. aureus* cells treated with C_{60}-GQD (200 μg/mL) in saline were covered with large amounts of particles, whereas those of cells treated similarly but with GO-GQD remain smooth as do those of cells in the controls, indicative of lack of particle-surface association. In contrast, *E. coli* cells retain smooth surfaces no matter which type of GQDs was used to treat them, as do those in the controls. Controls are those assayed similarly but without GQD addition. Scale bar = 500 nm. (c) AFM height (left) and tapping phase (right) images of *S. aureus* cells with and without C_{60}-GQD treatment, with the performance of GO-GQD treatment included as a reference. Scale bar = 50 nm.

positive bacteria, indicative of species-specific activity. To exclude the possibility that C_{60}-GQD is active against a specific *S. aureus* strain, we carry out similar assays but with another *S. aureus* strain (ATCC 29213, called *S. aureus* 2 throughout this work) and observed similar results (Figure 1a). Moreover, the observed activity of C_{60}-GQD against *S. aureus* is both dosage- (Figure S6) and time-dependent (Figure S7). Collectively, these results suggest that, in contrast to GO-GQDs, C_{60}-GQD is definitively bactericidal. What is noteworthy is that C_{60}-GQD exhibits species-specific activity, despite of the wide-spectrum activity of C_{60} dispersion.[15,24]

The as-observed distinction in activity profiles of C_{60}-GQD versus GO-GQDs and the species-specific activity of C_{60}-GQD are further confirmed with bacterial Dead/Live viability assays under fluorescence microscopy, using SYTO 9 and propidium iodide (PI)——two nucleic stains but with drastically different spectral characteristics and abilities to permeate healthy bacterial membranes——to label all and dead bacteria, respectively. Our results (Figure 1c) show that, after 3 h treatment with C_{60}-GQD, *S. aureus* cells stain intensely red, indicative of dead cells with compromised membranes, whereas cells of all other three bacteria (i.e., *E. coli*, *P. aeruginosa*, and *B. subtilis*) remain dark in the red channel, indicative of live cells with healthy membranes. In stark contrast, similar treatment but with GO-GQD makes cells of all four bacteria remain dark in the red channel, indicative of live cells. Consistent with the plate killing assays above, the bacterial Dead/Live viability assays confirm that C_{60}-GQD, in contrast to GO-GQDs, is definitively bactericidal and may be species-specific agent against *S. aureus*.

S. aureus is notorious for its ability to acquire antibiotic-resistance and cause high mortality rate.[25] Eradicating bacterial persisters, antibiotic-tolerant subpopulations,[26] may significantly impact emerging resistance,[27] as persistent presence of persisters effectively acts as a reservoir for resistant mutants.[26] Plate killing assays show that C_{60}-GQD (200 μg/mL) significantly reduces the viability ratio of *S. aureus* persisters (to 4.7%) but barely impacts that of *E. coli* persisters (Figure 1d), indicative of similar species-specific activity against persisters as against the wild-type counterparts (Figure 1a), suggesting the potential of C_{60}-GQD for applications as antibacterial agent in post antibiotic era.

C_{60}-GQD may be a species-specific agent against *S. aureus*, whereas GO-GQDs are completely inactive. A natural question to ask is "what accounts for this?" To address it, we first perform transmission electron microscopy (TEM) characterizations on bacterial cells with and without GQD treatment. Our results reveal that (Figure 2a), after 3 h treatment with C_{60}-GQD, surfaces of *S. aureus* cells exhibit many "tiny ticks/blebs", indicative of bacterial envelope disruption, whereas those of *E. coli* cells appear to be as smooth as those in control, indicative of lack of bacterial envelop disruption. In contrast, similar treatment but with GO-GQD barely impairs the bacterial surface smoothness for both *S. aureus* and *E. coli*, indicative of lack of bacterial envelop disruption. Taken together, these results suggest that both the distinct activity profiles of C_{60}-GQD versus GO-GQDs and the species-specific

DOI: 10.1021/acsami.5b10132
ACS Appl. Mater. Interfaces 2016, 8, 20−25

activity of C_{60}-GQD may be correlated with the ability of a GQD to disrupt the integrity of bacterial cell envelope.

Scanning electron microscopy (SEM) and atomic force microscopy (AFM) characterizations further suggest that the association of a GQD with a bacterial cell surface, the initial step for a GQD to disrupt bacterial cell envelope, may play critical roles in the observed distinction in activity profiles of C_{60}-GQD versus GO-GQDs and the species-specific activity of C_{60}-GQD. SEM images (Figure 2b and Figure S8) show that, after 3 h of treatment, *S. aureus* cells treated with C_{60}-GQD almost unanimously exhibit rough surfaces covered by particle-like features of 20−90 nm in size, whereas those treated with GO-GQD fail in doing so. In contrast to *S. aureus* cells, *E. coli* cells after GQD treatment appear to be similarly smooth as those in the control no matter whether GQD treatment is performed with C_{60}-GQD or GO-GQD. Clearly, both the distinct activity profiles of C_{60}-GQD versus GO-GQDs and the species-specific activity of C_{60}-GQD may correlate with the ability of a GQD to induce appearance of the particle-like features on surfaces of the target bacteria.

The particle-like features in SEM images should not be the projection of "ticks/blebs" observed under TEM, because those "ticks/blebs" are too small to be discerned under SEM. To affirm this speculation, we perform AFM characterizations on *S. aureus* cells with and without GQD treatment. Our AFM height images (Figure 2c, left) show that surfaces of *S. aureus* cells after C_{60}-GQD treatment appear to be significantly rough and covered with particle-like features of tens of nanometers in size whereas those after GO-GQD treatment are as smooth as those without GQD treatment, consistent with SEM results (Figure 2b). Moreover, AFM tapping phase images (Figure 2c, right) on *S. aureus* cells after C_{60}-GQD treatment differ significantly in phase (indicated by color) from those on *S. aureus* cells without any GQD treatment, as compared to the negligible difference in phase between *S. aureus* cell surfaces after GO-GQD treatment and those without any GQD treatment. In addition, phases of the particle-like features on *S. aureus* cells after C_{60}-GQD treatment differ significantly from those of intact *S. aureus* cell surfaces, indicative of their foreign-material origin. Collectively, these results suggest that the particle-like features of *S. aureus* cells observed in SEM images are adsorbed C_{60}-GQD particles, rather than bacteria blebs.

C_{60}-GQD inherits specific arrangement of hexagon and pentagon and thus nonzero Gaussian curvature from C_{60} cage, whereas GO-GQDs contain hexagon alone and thus have zero Gaussian and mean curvatures. On the basis of AFM characterizations (Figure S3) and SEM images (Figure 2b and Figure S8), we estimate the Gaussian curvature radii of C_{60}-GQD to be ∼313 nm on average and 210−548 nm in range (Please refer to the Supporting Information for details). On the other hand, *S. aureus* is a spherical bacterium with Gaussian curvature radii of ∼325 nm on average, whereas the other three bacteria tested in this work are rod-shaped with near zero Gaussian curvature surfaces along the long axis but nonzero, species-dependent Gaussian curvature around the end. Specifically, the end Gaussian curvature radii are ∼500 nm for *E. coli*,[28] ∼ 700 nm for *P. aeruginosa*,[29] and 500−1000 nm for *B. subtilis*.[30] Obviously, the Gaussian curvature radii of C_{60}-GQD are well-matched with those of *S. aureus*, but only slightly matched or mismatched with those of the other three bacteria above; in contrast to C_{60}-GQD, GO-GQD has surface curvature mismatch with all bacteria above. Combined with the antibacterial assays (Figure 1), these results suggest that surface curvature match between a GQD and a bacterium may correlate with the GQDs' antibacterial activities. Supportive evidence is found in the 14%-killing activity of C_{60}-GQD against *E. coli* (Figure 1a) which, in contrast to *B. subtilis* and *P. aeruginosa*, has end Gaussian curvature radii slightly matched with C_{60}-GQD (∼500 versus 210−548 nm) and end/total surface area ratio estimated to be of ∼30% (assuming an *E. coli* cell as a cylinder of 500 and 2000 nm in radius and length, respectively, plus two perfect hemispheres as the end-caps; overestimation may exist due to assumption of perfect geometry); the end/total surface area ratio of a rod-shaped bacterium may represent the probability of this bacterium to be killed by C_{60}-GQD, if its ends have Gaussian-curvature radii well matched with those of C_{60}-GQD and surface Gaussian-curvature match does correlate with bacterial-killing activity as we speculated. In fact, if we view both rod-shaped and spherical bacteria as two classes of rod-shaped objects that differ only in end/total surface area ratio (<100% versus exactly 100%), then C_{60}-GQD should be most potent (∼100% killing) against the spherical bacteria that have end Gaussian curvature radii well matched with C_{60}-GQD (210−548 nm). This is indeed the case with *S. aureus*; C_{60}-GQD kills >90% *S. aureus* indeed (Figure 1), very close to the ideal percentage (100%) as speculated. In similar vein, for a rod-shaped bacterium whose ends have Gaussian curvature radii (e.g., ∼300 nm) well-matched with those of C_{60}-GQD, the ideal percentage it can be killed by C_{60}-GQD may correspond to its end/total surface area ratio. Thus, surface Gaussian curvature match between a GQD and a target bacterium may determine whether the GQD can get associated with the target bacterial cell surface (Figure 3) to initiate the subsequent bactericidal envelope disruption processes, a similarly critical role curvature of carbon nanotube (CNT) plays in protein adsorption on CNT surface.[19] Unfortunately, how bacterial surface associated C_{60}-GQD disrupts the cell envelop integrity and consequently leads to cell death is unknown at the current stage.

Cytotoxicity to mammalian cells is a major concern in development of antibacterial agents. Our in vitro cell viability assays, using HepG2 as a representative human cell-line, show that C_{60}-GQD (50−200 μg/mL) barely impacts the viability of HepG2 cells both in saline and in serum-free DMEM (Figure S9a). Consistently, cell Dead/Live viability assays, which use SYTO 9 and PI to label all and dead cells, respectively, show that, after 4-h incubation with C_{60}-GQD in serum-free DMEM, HepG2 cells remain dark in the red channel, indicative of live cells (Figure S9b). Collectively, these results consistently suggest that C_{60}-GQD may lack cytotoxicity to mammalian cells. Note that both GO-GQD[31] and spherical carbon nanodot[32] lack toxicity even when administered in vivo. It is thus reasonable to expect that C_{60}-GQD, which have similar chemical compositions as them, may also lack toxicity in vivo. With species-specific antibacterial activity and low/no cytotoxicity, C_{60}-GQD may have implications in "personalized healthcare" in post antibiotic era.[33]

In summary, we find that although GO-GQDs unanimously lack antibacterial property, C_{60}-GQD exhibits species-specific activity against *Staphylococcus aureus* (*S. aureus*), including the antibiotic-tolerant persisters. The observed activity may correlate with a GQD's ability to disrupt bacterial cell envelop integrity, and surface Gaussian curvature match between a GQD and a target bacterium may play pivotal role in determining whether the GQD can get associated with cell surface of the target bacterium, to initiate the subsequent

DOI: 10.1021/acsami.5b10132
ACS Appl. Mater. Interfaces 2016, 8, 20−25

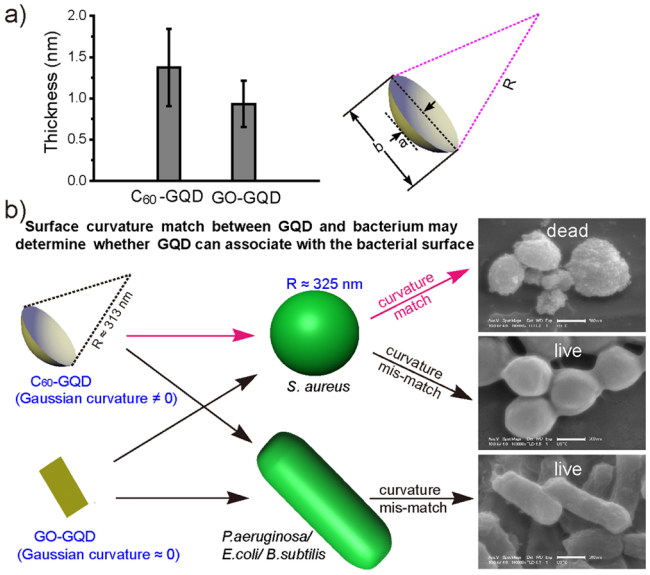

Figure 3. (a) (Left) According to AFM height profiles of GQDs, the average apparent sheet thicknesses of C_{60}-GQD and GO-GQD are 1.37 ± 0.46 and 0.94 ± 0.29 nm, respectively. (Right) We estimate the Gaussian curvature radii of C_{60}-GQD, *R*, using the equation of $R^2 = (R - a)^2 + (b/2)^2$, where *a* and *b* are the relative enhancement in sheet thickness conferred by curvature and the sheet diameter, respectively. We estimate *a* for C_{60}-GQD to be ∼1 nm on average (with range of 0.57−1.49 nm), by subtracting the apparent sheet thickness obtained with its AFM height profiles characterizations (i.e., 1.37 ± 0.46 nm) with the theoretical thickness of a single layer of carbon atoms (i.e., ∼ 0.34 nm). According to SEM images on C_{60}-GQD adsorbed on *S. aureus* surface, we estimate the average sheet diameter, b, to be ∼50 nm. As a result, the Gaussian curvature radii of C_{60}-GQD are estimated to be ∼313 nm on average and 210−548 nm in range. (b) Schematic illustration on how surface curvature match between a GQD and a target bacterium surface may be correlated with the GQD's antibacterial property. C_{60}-GQD has Gaussian curvature radii of ∼313 nm, whereas GO-GQD has zero Gaussian curvature because of its sheet morphology; *S. aureus* is a spherical bacterium with Gaussian curvature radii of ∼325 nm on average, whereas the other three tested bacteria (i.e., *E. coli*, *P. aeruginosa*, and *B. subtilis*) are rod-shaped.

bactericidal envelope destabilization processes. Similar as GO-GQD, C_{60}-GQD lacks cytotoxicity to mammalian cells. This work highlights the importance of both fingerprint difference in structure of GQDs' source materials and bacterial cell shapes in GQDs' antibacterial property and suggests potential of C_{60}-GQD for applications as antimicrobials in "personalized healthcare" in the post antibiotic era.

■ ASSOCIATED CONTENT

Supporting Information

The Supporting Information is available free of charge on the ACS Publications website at DOI: 10.1021/acsami.5b10132.

Figure S1−S9, Table S1, additional Results and Discussion, and Materials and Methods (PDF)

■ AUTHOR INFORMATION

Corresponding Author

*E-mail: lhyang@ustc.edu.cn. Tel: (86)551 6360 6960.

Notes

The authors declare no competing financial interest.

■ ACKNOWLEDGMENTS

We greatly thank Professor Jun Wang at USTC for use of their facilities and Professor Hangxun Xu for helpful discussion. UV−vis spectroscopy, FT-IR spectrum, and fluorescence spectrum characterizations were carried out in the Analytical Center of School of Chemistry and Materials Science at USTC. This work was supported in part by the National Natural Science Foundation of China (21174138, L.Y.; 51322204, Y.Z.), Ministry of Education of the People's Republic of China (NCET-13-0547, WK2060200012, L.Y.; NCET-12-0516, WK2060140014, WK2060140017, Y.Z.), China Government 1000 Plan Talent Program (Y.Z.), Chinese Academy of Sciences (the Youth Innovation Promotion Association, L.Y.; the External Cooperation Program of BIC via 211134KYSB20130017, Y.Z.), and the Natural Science Foundation of Anhui Province (1308085QB28, L.Y.).

■ REFERENCES

(1) Li, L.-s.; Yan, X. Colloidal Graphene Quantum Dots. *J. Phys. Chem. Lett.* **2010**, *1*, 2572−2576.
(2) Bacon, M.; Bradley, S. J.; Nann, T. Graphene Quantum Dots. *Part. Part. Syst. Charact.* **2014**, *31*, 415−428.
(3) Trauzettel, B.; Bulaev, D. V.; Loss, D.; Burkard, G. Spin Qubits in Graphene Quantum Dots. *Nat. Phys.* **2007**, *3*, 192−196.
(4) Ritter, K. A.; Lyding, J. W. The Influence of Edge Structure on the Electronic Properties of Graphene Quantum Dots and Nanoribbons. *Nat. Mater.* **2009**, *8*, 235−242.
(5) Pan, D.; Zhang, J.; Li, Z.; Wu, M. Hydrothermal Route for Cutting Graphene Sheets into Blue-Luminescent Graphene Quantum Dots. *Adv. Mater.* **2010**, *22*, 734−738.
(6) Wang, L.; Zhu, S. J.; Wang, H. Y.; Qu, S. N.; Zhang, Y. L.; Zhang, J. H.; Chen, Q. D.; Xu, H. L.; Han, W.; Yang, B.; Sun, H. B. Common Origin of Green Luminescence in Carbon Nanodots and Graphene Quantum Dots. *ACS Nano* **2014**, *8*, 2541−2547.
(7) Ye, R. Q.; Xiang, C. S.; Lin, J.; Peng, Z. W.; Huang, K. W.; Yan, Z.; Cook, N. P.; Samuel, E. L. G.; Hwang, C. C.; Ruan, G. D.; Ceriotti, G.; Raji, A. R. O.; Marti, A. A.; Tour, J. M. Coal as an Abundant Source of Graphene Quantum Dots. *Nat. Commun.* **2013**, *4*, 2943.
(8) Peng, J.; Gao, W.; Gupta, B. K.; Liu, Z.; Romero-Aburto, R.; Ge, L. H.; Song, L.; Alemany, L. B.; Zhan, X. B.; Gao, G. H.; Vithayathil, S. A.; Kaipparettu, B. A.; Marti, A. A.; Hayashi, T.; Zhu, J. J.; Ajayan, P. M. Graphene Quantum Dots Derived from Carbon Fibers. *Nano Lett.* **2012**, *12*, 844−849.
(9) Chua, C. K.; Sofer, Z.; Simek, P.; Jankovsky, O.; Klimova, K.; Bakardjieva, S.; Kuckova, S. H.; Pumera, M. Synthesis of Strongly Fluorescent Graphene Quantum Dots by Cage-Opening Buckminsterfullerene. *ACS Nano* **2015**, *9*, 2548−2555.
(10) Chen, G.; Zhuo, Z.; Ni, K.; Kim, N. Y.; Zhao, Y.; Chen, Z.; Xiang, B.; Yang, L.; Zhang, Q.; Lee, Z.; Wu, X.; Ruoff, R. S.; Zhu, Y. Rupturing C60 Molecules into Graphene-Oxide-Like Quantum Dots: Structure, Photoluminescence and Catalytic Application. *Small* **2015**, *11*, 5296.
(11) Tang, L.; Ji, R.; Cao, X.; Lin, J.; Jiang, H.; Li, X.; Teng, K. S.; Luk, C. M.; Zeng, S.; Hao, J.; Lau, S. P. Deep Ultraviolet Photoluminescence of Water-Soluble Self-Passivated Graphene Quantum Dots. *ACS Nano* **2012**, *6*, 5102−5110.
(12) Yan, X.; Li, B.; Li, L.-s. Colloidal Graphene Quantum Dots with Well-Defined Structures. *Acc. Chem. Res.* **2013**, *46*, 2254−2262.
(13) Hu, W.; Peng, C.; Luo, W.; Lv, M.; Li, X.; Li, D.; Huang, Q.; Fan, C. Graphene-Based Antibacterial Paper. *ACS Nano* **2010**, *4*, 4317−4323.
(14) Kang, S.; Pinault, M.; Pfefferle, L. D.; Elimelech, M. Single-Walled Carbon Nanotubes Exhibit Strong Antimicrobial Activity. *Langmuir* **2007**, *23*, 8670−8673.
(15) Lyon, D. Y.; Brunet, L.; Hinkal, G. W.; Wiesner, M. R.; Alvarez, P. J. J. Antibacterial Activity of Fullerene Water Suspensions (nC_{60}) Is Not Due to Ros-Mediated Damage. *Nano Lett.* **2008**, *8*, 1539−1543.

DOI: 10.1021/acsami.5b10132
ACS Appl. Mater. Interfaces 2016, 8, 20−25

(16) Sun, H. J.; Gao, N.; Dong, K.; Ren, J. S.; Qu, X. G. Graphene Quantum Dots-Band-Aids Used for Wound Disinfection. *ACS Nano* **2014**, *8*, 6202−6210.
(17) Perreault, F.; de Faria, A. F.; Nejati, S.; Elimelech, M. Antimicrobial Properties of Graphene Oxide Nanosheets: Why Size Matters. *ACS Nano* **2015**, *9*, 7226−7236.
(18) Ristic, B. Z.; Milenkovic, M. M.; Dakic, I. R.; Todorovic-Markovic, B. M.; Milosavljevic, M. S.; Budimir, M. D.; Paunovic, V. G.; Dramicanin, M. D.; Markovic, Z. M.; Trajkovic, V. S. Photodynamic Antibacterial Effect of Graphene Quantum Dots. *Biomaterials* **2014**, *35*, 4428−4435.
(19) Gu, Z. L.; Yang, Z. X.; Chong, Y.; Ge, C. C.; Weber, J. K.; Bell, D. R.; Zhou, R. H. Surface Curvature Relation to Protein Adsorption for Carbon-Based Nanomaterials. *Sci. Rep.* **2015**, *5*, 10886.
(20) Eda, G.; Lin, Y.-Y.; Mattevi, C.; Yamaguchi, H.; Chen, H.-A.; Chen, I. S.; Chen, C.-W.; Chhowalla, M. Blue Photoluminescence from Chemically Derived Graphene Oxide. *Adv. Mater.* **2010**, *22*, 505−509.
(21) Hui, L.; Piao, J.-G.; Auletta, J.; Hu, K.; Zhu, Y.; Meyer, T.; Liu, H.; Yang, L. Availability of the Basal Planes of Graphene Oxide Determines Whether It Is Antibacterial. *ACS Appl. Mater. Interfaces* **2014**, *6*, 13183−13190.
(22) Tu, Y.; Lv, M.; Xiu, P.; Huynh, T.; Zhang, M.; Castelli, M.; Liu, Z.; Huang, Q.; Fan, C.; Fang, H.; Zhou, R. Destructive Extraction of Phospholipids from Escherichia Coli Membranes by Graphene Nanosheets. *Nat. Nanotechnol.* **2013**, *8*, 594−601.
(23) Liu, S. B.; Hu, M.; Zeng, T. H.; Wu, R.; Jiang, R. R.; Wei, J.; Wang, L.; Kong, J.; Chen, Y. Lateral Dimension-Dependent Antibacterial Activity of Graphene Oxide Sheets. *Langmuir* **2012**, *28*, 12364−12372.
(24) Lyon, D. Y.; Adams, L. K.; Falkner, J. C.; Alvarez, P. J. J. Antibacterial Activity of Fullerene Water Suspensions: Effects of Preparation Method and Particle Size. *Environ. Sci. Technol.* **2006**, *40*, 4360−4366.
(25) Chambers, H. F.; DeLeo, F. R. Waves of Resistance: Staphylococcus Aureus in the Antibiotic Era. *Nat. Rev. Microbiol.* **2009**, *7*, 629−641.
(26) Lewis, K. Persister Cells, Dormancy and Infectious Disease. *Nat. Rev. Microbiol.* **2007**, *5*, 48−56.
(27) Schmidt, N. W.; Deshayes, S.; Hawker, S.; Blacker, A.; Kasko, A. M.; Wong, G. C. L. Engineering Persister-Specific Antibiotics with Synergistic Antimicrobial Functions. *ACS Nano* **2014**, *8*, 8786−8793.
(28) Renner, L. D.; Weibel, D. B. Cardiolipin Microdomains Localize to Negatively Curved Regions of Escherichia Coli Membranes. *Proc. Natl. Acad. Sci. U. S. A.* **2011**, *108*, 6264−6269.
(29) Roosjen, A.; Busscher, H. J.; Nordel, W.; van der Mei, H. C. Bacterial Factors Influencing Adhesion of Pseudomonas Aeruginosa Strains to a Poly(Ethylene Oxide) Brush. *Microbiology* **2006**, *152*, 2673−2682.
(30) Wasnik, V.; Wingreen, N. S.; Mukhopadhyay, R. Modeling Curvature-Dependent Subcellular Localization of the Small Sporulation Protein Spovm in Bacillus Subtilis. *PLoS One* **2015**, *10*, e0111971.
(31) Chong, Y.; Ma, Y.; Shen, H.; Tu, X.; Zhou, X.; Xu, J.; Dai, J.; Fan, S.; Zhang, Z. The In vitro and In vivo Toxicity of Graphene Quantum Dots. *Biomaterials* **2014**, *35*, 5041−5048.
(32) Huang, X.; Zhang, F.; Zhu, L.; Choi, K. Y.; Guo, N.; Guo, J.; Tackett, K.; Anilkumar, P.; Liu, G.; Quan, Q.; Choi, H. S.; Niu, G.; Sun, Y.-P.; Lee, S.; Chen, X. Effect of Injection Routes on the Biodistribution, Clearance, and Tumor Uptake of Carbon Dots. *ACS Nano* **2013**, *7*, 5684−5693.
(33) Perros, M. A Sustainable Model for Antibiotics. *Science* **2015**, *347*, 1062−1064.

DOI: 10.1021/acsami.5b10132
ACS Appl. Mater. Interfaces 2016, 8, 20−25